GW Detectors Principia

Block 2: Experimental Fundamentals

Gianluca Gemme

INFN — Sezione di Genova
Virgo and ET Collaborations

STGWD 2026 — PhD International School on Technologies in Gravitational Waves Detection

Outline of Block 2

A. From theory to instrument
   - Scale of the problem, Michelson basics
   - Shot-noise-limited sensitivity of a simple Michelson

B. Why real detectors are not plain Michelsons
   - Fabry-Perot arm cavities, power and signal recycling
   - Squeezing (pointer only)

C. Noise budget — the fundamentals
   - Seismic, Newtonian, thermal, quantum
   - Reading a real sensitivity curve

D. Network, reach, and what comes next

Recap from Block 1 — what do we need to measure?

From Block 1, the detector output is

$$h(t) = \frac{\Delta L_x(t) - \Delta L_y(t)}{L} = F_+ h_+ + F_\times h_\times .$$

- In the long-wavelength regime, the GW acts as a quadrupolar tidal force on the test masses.
- Light propagation in TT gauge produces audio sidebands of amplitude $\propto h_0 k_L L$ around the laser carrier.
- Our job: turn a differential length change at the 10^{-18} m level into a measurable optical signal.

The core question of Block 2

How do we build an instrument with strain sensitivity $\sim 10^{-23}/\sqrt{\mathrm{Hz}}$ between 10 Hz and 10 kHz?

A. The scale of the problem

- Typical GW strain from a compact binary coalescence at ~ 100 Mpc: $h \sim 10^{-21}$.
- Arm length $L \sim$ few km:

$$\Delta L \sim 10^{-18}\ \mathrm{m}.$$

- Compare with:
  - classical proton radius: $\sim 10^{-15}$ m;
  - atomic nucleus: $\sim 10^{-14}$ m.
- We need to measure ΔL **three orders of magnitude smaller than a nucleus**, over a 3 km arm.

Why interferometry, why differential

- **Interferometry** converts a length change into a phase shift of the light:

$$\Delta\varphi = k_L\,\Delta L = \frac{2\pi\,\Delta L}{\lambda_L} \sim 10^{-11}\ \mathrm{rad}$$

  (for $\lambda_L = 1064$ nm, $\Delta L = 10^{-18}$ m).
- **Differential** measurement (two arms, orthogonal):
  - doubles the signal: GW stretches one arm and squeezes the other;
  - common-mode rejects laser frequency fluctuations, common vibrations, and temperature drifts.
- A Michelson interferometer is the simplest topology that realizes both ideas.

The Michelson interferometer — layout

- Laser at input, beam splitter in the centre.
- Two arms along $\hat{x}$ and $\hat{y}$, end mirrors at distance L.
- Interference at the beam splitter on return.
- Two output ports:
  - symmetric (back to laser);
  - antisymmetric (photodiode).
- Tuning the microscopic arm-length difference chooses the interference condition.

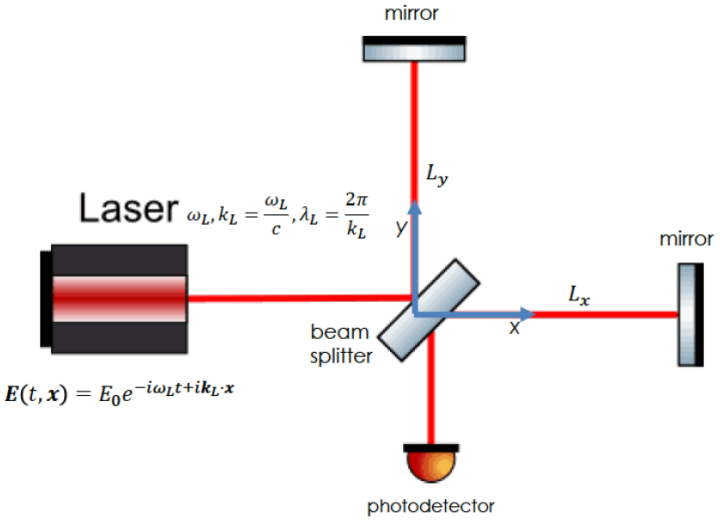

Figure: Michelson schematic: laser, BS, two arms, photodiode at AS port.

Output field vs. arm-length difference

Let the beam splitter have amplitude reflectivity $r = 1/\sqrt{2}$ and transmissivity $t = 1/\sqrt{2}$. Propagating input field $E_{\rm in} = E_0 e^{-i\omega_L t}$ through both arms and recombining at the beam splitter, the field at the antisymmetric port is

$$E_{\rm AS}(t) = -\tfrac{1}{2}\, E_0\, e^{-i\omega_L t}\left(e^{2ik_L L_x} - e^{2ik_L L_y}\right).$$

Power on the photodiode:

$$P_{\rm AS} = \tfrac{1}{2}\, P_{\rm in}\left[1 - \cos\left(2k_L(L_x - L_y)\right)\right].$$

- Sinusoidal in the differential arm length.
- Maxima at bright fringe, zeros at *dark fringe*: $k_L(L_x - L_y) = n\pi$.

The fringe and dark-fringe operation

- Working point: near the dark fringe, $P_{\mathrm{AS}} \to 0$.
- Linearized response around dark fringe for small $\delta L = L_x - L_y - L_{\mathrm{DC}}$:

$$P_{\mathrm{AS}} \simeq P_{\mathrm{in}} \, (k_L \, \delta L)^2 .$$

  Quadratic: insensitive to small δL, bad.
- Solution: small offset from dark fringe *or*, better, a heterodyne/DC-readout scheme.
- In real detectors the output is *not* the raw AS power — it is a demodulated signal built on top of RF sidebands or a small DC bias. Concept only here.

→ *Optimal detection strategies:* ***D. Bersanetti*** *— Interferometer Controls (Sat 23).*

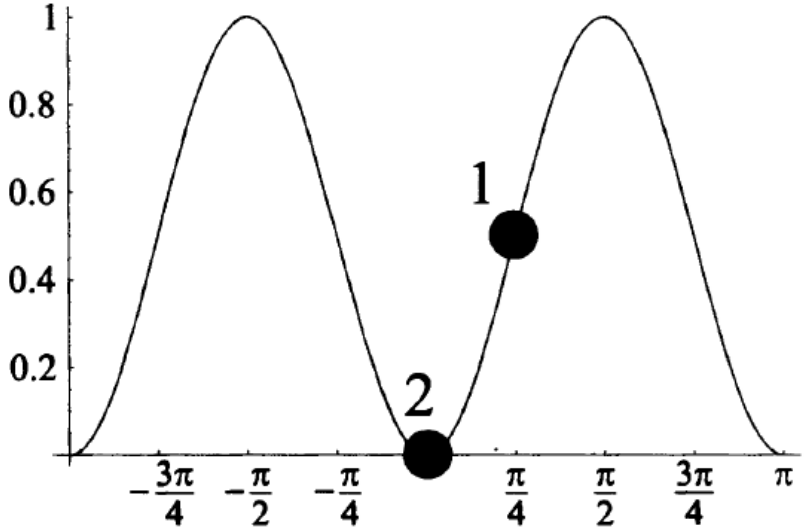

Figure: Fringe curve $P_{\phi/P_{in}}(\delta L)$ with working point(s) indicated. CREDIT [1]

GW-induced phase shift

A GW with amplitude $h(t)$ applied to the differential arm length gives, from Block 1,

$$L_x - L_y \;\rightarrow\; L_x - L_y + L\,h(t).$$

The resulting phase shift is

$$\Delta\varphi_{\rm gw}(t) = 2k_L L\,h(t) = \frac{4\pi L}{\lambda_L}\,h(t).$$

Key equation

$\Delta\varphi_{\rm gw} \propto L \cdot h$ — phase scales linearly with arm length.

- Longer arms $\Rightarrow$ larger phase shift.
- But beyond $L \sim \lambda_{\rm gw}/2$ the sinc factor starts to kill the response (Block 1).
- For ground detectors this suggests L in the few-km range — the rest is technology.

Audio sidebands at the output (link to Block 1)

Combining the round-trip calculation of Block 1 with the Michelson recombination:

- The carrier at ω_L is suppressed at the dark port.
- Audio sidebands at $\omega_L \pm \omega_{\rm gw}$ pass through.
- Their amplitude is proportional to $h_0\, k_L L\, \mathrm{sinc}(\omega_{\rm gw} L/c)$.
- The photodiode detects the beat between carrier (reintroduced by a small DC offset or by RF sidebands) and signal sidebands, producing a photocurrent $\propto h(t)$.

Consequence

The interferometer is a linear, frequency-dependent transducer from $h(t)$ to photocurrent.

Shot-noise-limited Michelson — order of magnitude

Shot noise on the photodiode sets a minimum detectable phase:

$$\Delta\varphi_{\rm shot} \simeq \sqrt{\frac{\hbar\omega_L}{P_{\rm in}}} \quad [\mathrm{rad}/\sqrt{\mathrm{Hz}}].$$

Converting to strain using $\Delta\varphi_{\rm gw} = (4\pi L/\lambda_L)\, h$:

$$h_{\rm shot}(f) \simeq \frac{1}{L}\sqrt{\frac{\hbar c\lambda_L}{2\pi P_{\rm in}}} \quad [1/\sqrt{\mathrm{Hz}}].$$

- For $L = 3$ km, $\lambda_L = 1064$ nm, $P_{\rm in} = 10$ W: $h_{\rm shot} \sim 10^{-20}/\sqrt{\mathrm{Hz}}$.
- Two orders of magnitude short of the target.
- **Solution**: increase effective L (Fabry-Perot), increase circulating power (power recycling), reduce vacuum noise (squeezing).

B. Two ways to improve: more photons, longer path

From the shot-noise formula:

$$h_{\mathrm{shot}} \propto \frac{1}{L\sqrt{P_{\mathrm{in}}}}.$$

Two independent handles:

1. **Increase the effective optical path** seen by the light.
   $\Rightarrow$ Fabry-Perot arm cavities.
2. **Increase the circulating optical power**.
   $\Rightarrow$ Power recycling.

Both are part of every advanced detector. Plus:

- **Signal recycling**: reshape the frequency response.
- **Squeezing**: beat the shot-noise limit.

Fabry-Perot arm cavities

- Replace each arm with a resonant Fabry-Perot cavity.
- Light bounces many times $\Rightarrow$ effective arm length multiplied by finesse:

$$L_{\rm eff} \simeq \frac{2\mathcal{F}}{\pi} L.$$

- For $L = 3$ km, $\mathcal{F} \simeq 450 \Rightarrow L_{\rm eff} \sim 10^3$ km.
- **Trade-off**: bandwidth limited by the cavity pole

$$f_{\rm pole} = \frac{c}{4\mathcal{F}L} \sim 50 \text{ Hz}.$$

- Response flat up to $f_{\rm pole}$, then rolls off as $1/f$.

$\rightarrow$ *Full optical layout:* ***A. Perreca*** *— Optical configurations (Fri 22 & Sat 23).*

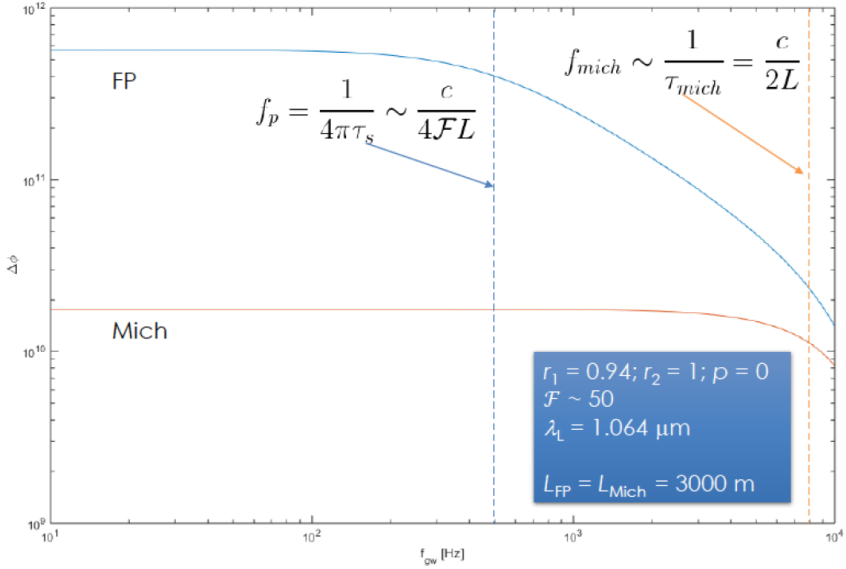

Figure: FP-Michelson layout; response vs frequency with cavity pole.

Power recycling

- At dark fringe, all the input power is reflected back toward the laser.
- Place a partially-transmitting mirror (PRM) at the symmetric port: forms a cavity with the rest of the interferometer.
- Result: input power is *recycled*, circulating power increases by the recycling gain

$$G_{\mathrm{PR}} \sim \frac{1}{1 - r_{\mathrm{PRM}}\, r_{\mathrm{ITF}}}.$$

- Typical gain $G_{\mathrm{PR}} \sim 40$–50 for advanced detectors.
- Enters shot noise as $\sqrt{G_{\mathrm{PR}}}$.

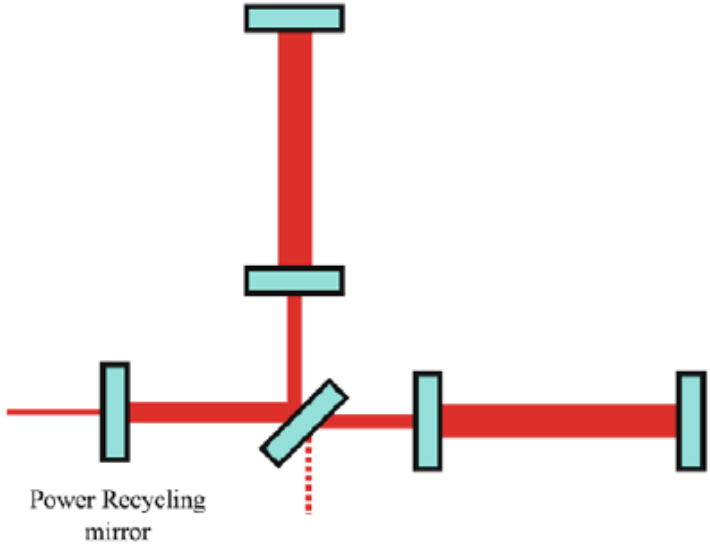

Figure: Optical layout with PRM, arm cavities, BS, AS port.

Signal recycling — concept

- Add a partially-transmitting mirror (SRM) at the antisymmetric port.
- Forms a cavity for the *signal sidebands*.
- Does not affect the carrier (which is dark).
- Two regimes:
  - resonant (signal recycling): narrow-band gain;
  - detuned: tunable peak in the sensitivity.
- Allows reshaping the sensitivity curve around the targeted astrophysical sources.

→ *Full treatment:* ***A. Perreca*** *— Optical configurations (Fri 22 & Sat 23). Controls:* ***D. Bersanetti*** *— Interferometer controls (Sat 23).*

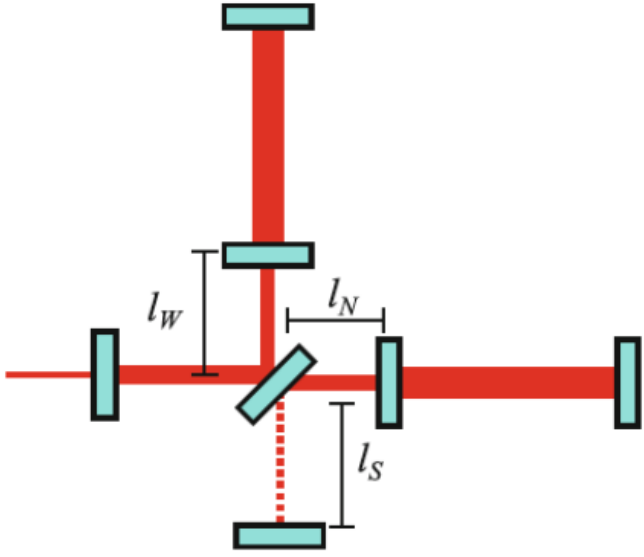

Figure: Dual-recycled Michelson layout with PRM and SRM.

Squeezing — a one-slide pointer

- The shot-noise floor is set by the *vacuum fluctuations* of the electromagnetic field entering the antisymmetric port.
- A squeezed vacuum state has reduced fluctuations in one quadrature, at the expense of increased fluctuations in the other.
- Inject it at the AS port:
  - **Frequency-independent** squeezing: reduces shot noise but increases radiation-pressure noise.
  - **Frequency-dependent** squeezing: uses a filter cavity to rotate the squeezing angle, reducing *both* at once.
- Routinely implemented in O4; gains of a few dB across the detection band.
- → ***F. Sorrentino*** *— Squeezing (Tue 26, 09:00) for the full treatment, including filter cavities and frequency-dependent squeezing.*

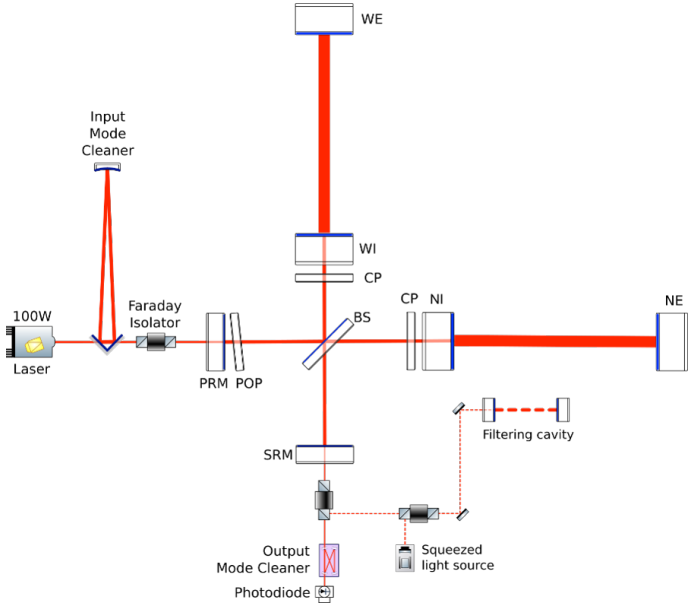

Figure: Fabry-Pérot layout with Power and Signal Recycling and Frequency Dependent Squeezing.

C. Two design principles for a GW detector

1. The test masses must be **quieter than the signal** you want to observe.
2. The test-mass position must be **read out with the required accuracy** — without introducing unacceptable back-action noise.

Consequences

- (1) drives the mechanical design: suspensions, seismic isolation, low-loss materials, vacuum.
- (2) drives the optical design: high power, dark fringe, squeezing, quantum-non-demolition techniques.

The sensitivity curve as a map of the detector

The strain sensitivity $\sqrt{S_h(f)}$ $[1/\sqrt{\mathrm{Hz}}]$ is the essential figure of merit.

Characteristic shape (advanced detectors):

- **Low** f ($\lesssim 10$ Hz): seismic + Newtonian noise. Steep wall.
- **Mid** f (10–300 Hz): thermal noise + radiation pressure. Bucket region.
- **High** f ($\gtrsim 300$ Hz): shot noise. $\sim$ flat or slowly rising.

Each frequency decade is limited by a *different* physics.

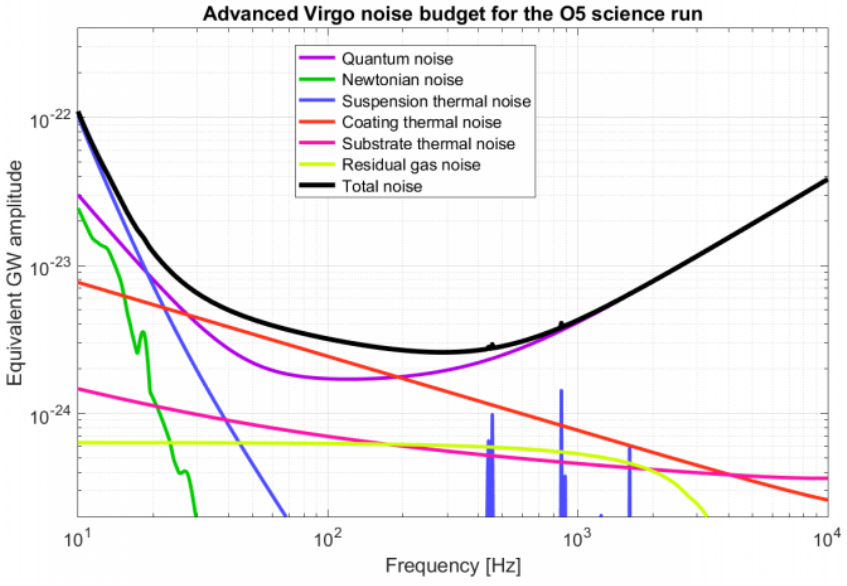

Figure: AdV noise budget (theory).

Seismic noise — source and spectrum

- Continuous, non-stationary ground motion.
- Sources:
  - natural: microseism from ocean waves (0.1–0.5 Hz), wind, earthquakes, tides;
  - anthropogenic: traffic, industry, agriculture.
- Typical ground displacement spectrum:

$$x_{\mathrm{seis}}(f) \sim 10^{-7} \left(\frac{1\ \mathrm{Hz}}{f}\right)^2\ \mathrm{m}/\sqrt{\mathrm{Hz}}$$

  above a few Hz.
- Compare with target $\sim 10^{-19}\ \mathrm{m}/\sqrt{\mathrm{Hz}}$: need **12 orders of magnitude** of attenuation.

→ *Isolation systems:* ***P. Chessa*** *— Seismic filtering (Fri 22, 11:05). Cryogenic regime:* ***E. Majorana*** *— Cryogenics in GW detectors (Wed 27, 11:05).*

Seismic isolation — the pendulum principle

A pendulum of natural frequency f_0 acts as a low-pass filter for horizontal ground motion:

$$\frac{x_{\mathrm{mass}}}{x_{\mathrm{ground}}} \simeq \left(\frac{f_0}{f}\right)^2 \quad \text{for } f \gg f_0.$$

- Single pendulum at $f_0 \sim 0.5$ Hz: $\sim$40 dB at 10 Hz.
- Multi-stage (cascade of N pendulums): $\sim 20N \log(f/f_0)$ dB.
- Virgo *superattenuator*: 6 stages, $>$200 dB isolation above 10 Hz.

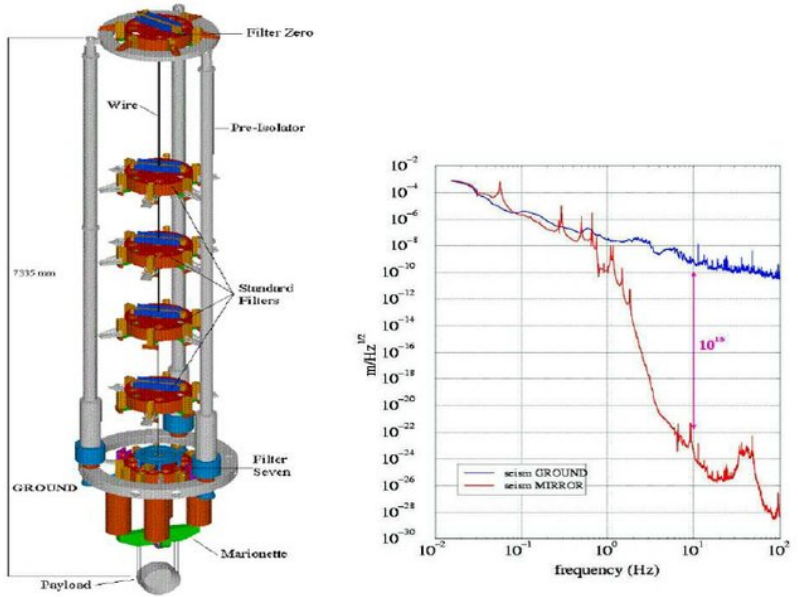

Figure: Multi-stage pendulum / superattenuator schematic.

Newtonian (gravity-gradient) noise — concept

- Density fluctuations in the ground and atmosphere around the test masses produce fluctuating *Newtonian gravitational forces* on the masses.
- Dominant sources:
  - seismic density waves (Rayleigh, body waves) in the ground;
  - atmospheric infrasound and pressure fluctuations.
- Impossible to shield gravitationally $\Rightarrow$ fundamental low-frequency wall at a surface site.
- Mitigation:
  - **Site selection**: quiet, low-population areas.
  - **Underground**: gravity gradients from surface sources are attenuated.
  - **Noise subtraction**: seismometer arrays measure the sources and subtract their effect.

Thermal noise — fluctuation-dissipation theorem

Any mechanical system that dissipates energy also generates noise. For a harmonic oscillator with mass m, resonance frequency ω_0 and quality factor Q:

$$S_x(\omega) = \frac{4k_B T\, \omega_0/Q}{m\left[(\omega^2 - \omega_0^2)^2 + (\omega\omega_0/Q)^2\right]}.$$

- Amplitude depends on the *loss angle*, not on the response function alone.
- Off resonance: noise is small *if Q is high* (low loss).
- Design rule: use low-loss materials (fused silica, sapphire, silicon).

Low mechanical losses $\Rightarrow$ low thermal noise off resonance.

Suspension thermal noise

- Final stage of the suspension: mirror hung by thin fibres.
- Pendulum mode at ~ 0.6 Hz; violin modes at ~ 400 Hz, 800 Hz, ...
- Thermal noise contributes mostly off-resonance: **steeply falling** with f (due to high Q).
- Mitigation:
  - monolithic silica fibres ($Q \sim 10^8$);
  - cryogenic suspensions (KAGRA, ET-LF);
  - longer, thinner fibres (within mechanical tolerance).

→ ***P. Chessa*** — *Seismic filtering (Fri 22, 11:05);* ***E. Majorana*** — *Cryogenics (Wed 27, 11:05);* ***I. Nardecchia*** — *Thermal compensation (Mon 25, 14:30).*

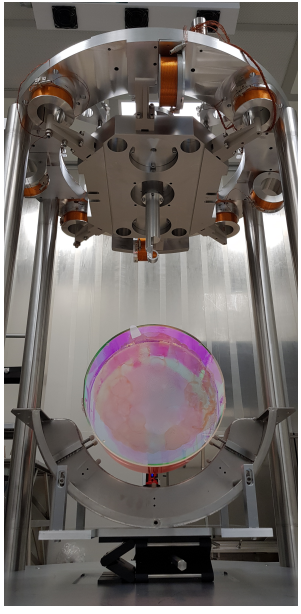

Figure: Monolithic final stage: mirror + silica fibres + marionette.

Mirror and coating thermal noise

- Two contributions:
  - **Substrate** Brownian noise (internal friction of the bulk material);
  - **Coating** Brownian noise (internal friction of the dielectric stack).
- Coating thermal noise is *dominant* at mid-frequencies in advanced detectors.
- Drivers:
  - coating mechanical loss angle ϕ_c;
  - coating thickness;
  - beam size on the mirror (larger spot $\Rightarrow$ less noise, averaging over more material).
- Mitigation: low-loss coating materials (titania-doped silica, amorphous silicon), larger spots, cryogenic operation.

$\rightarrow$ ***M. Magnozzi*** *— Coatings & Materials (Fri 22, 14:30);* ***E. Majorana*** *— Cryogenics (Wed 27, 11:05);* ***I. Nardecchia*** *— Thermal compensation (Mon 25, 14:30).*

Quantum noise — overview

Two contributions, both quantum:

- Shot noise (photon counting statistics at the photodiode)

$$h_{\mathrm{shot}}(f) \propto \frac{1}{\sqrt{P}}$$

  $\Rightarrow$ dominant at **high frequency**.

- Radiation-pressure noise (photon momentum kicks on the mirrors)

$$h_{\mathrm{rp}}(f) \propto \frac{\sqrt{P}}{m\, f^2}$$

  $\Rightarrow$ dominant at **low frequency**.

Shot noise — scaling with power and frequency

$$\sqrt{S_h^{\mathrm{shot}}(f)} = \frac{1}{L}\sqrt{\frac{\hbar c \lambda_L}{2\pi P_{\mathrm{circ}}}}\sqrt{1+(f/f_{\mathrm{pole}})^2}.$$

- Decreases as $1/\sqrt{P_{\mathrm{circ}}}$ $\Rightarrow$ motivates power recycling + high-power lasers.
- Rises above the cavity pole as f: this is why the high-frequency wing of the curve tilts upward.
- Can be beaten below the vacuum limit using squeezing.

Shot noise is the only noise we can fight *by turning up the laser*.

Radiation-pressure noise — scaling

$$\sqrt{S_h^{\mathrm{rp}}(f)} = \frac{1}{mL\,(2\pi f)^2}\,\sqrt{\frac{8\pi\hbar P_{\mathrm{circ}}}{c\lambda_L}}.$$

- Rises as $P^{1/2}$ $\Rightarrow$ the price we pay for high laser power.
- Falls as $1/f^2$ $\Rightarrow$ matters only at low f.
- Mitigation: **heavier mirrors** (Virgo 42 kg, LIGO 40 kg, ET target 200 kg).
- Or: frequency-dependent squeezing (Block 2 slide 16).

Shot noise and radiation-pressure noise push in opposite directions for P — their sum defines an optimum.

Standard Quantum Limit — concept

The sum of shot and radiation-pressure noise has a minimum at each frequency, the Standard Quantum Limit (SQL):

$$S_h^{\mathrm{SQL}}(f) = \frac{8\hbar}{mL^2\,(2\pi f)^2}.$$

- Reached by choosing the optimal circulating power at each frequency.
- In practice: fixed $P \Rightarrow$ SQL touched at one frequency only.
- The SQL *can* be beaten using **quantum-non-demolition** techniques (FD squeezing, speed-meter topologies, . . .).
- Detailed treatment: specialized lecture.

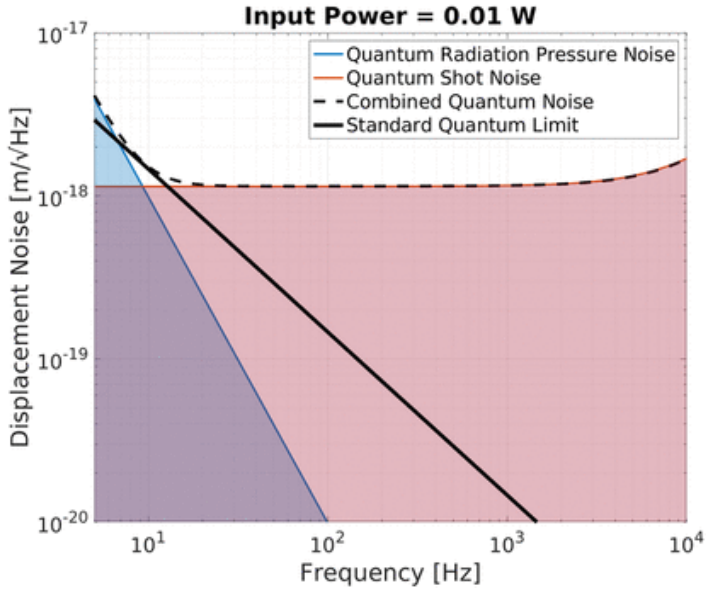

Figure: Shot + RP components and their sum vs frequency; SQL envelope.

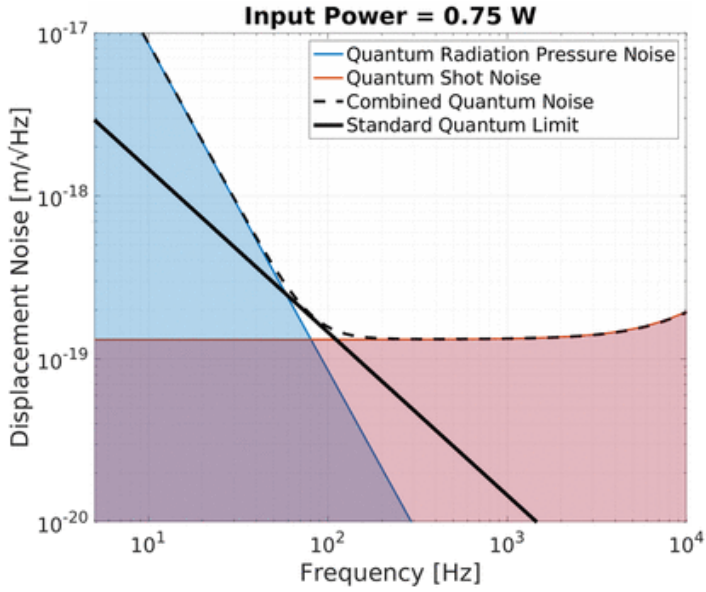

Figure: Shot + RP components and their sum vs frequency; SQL envelope.

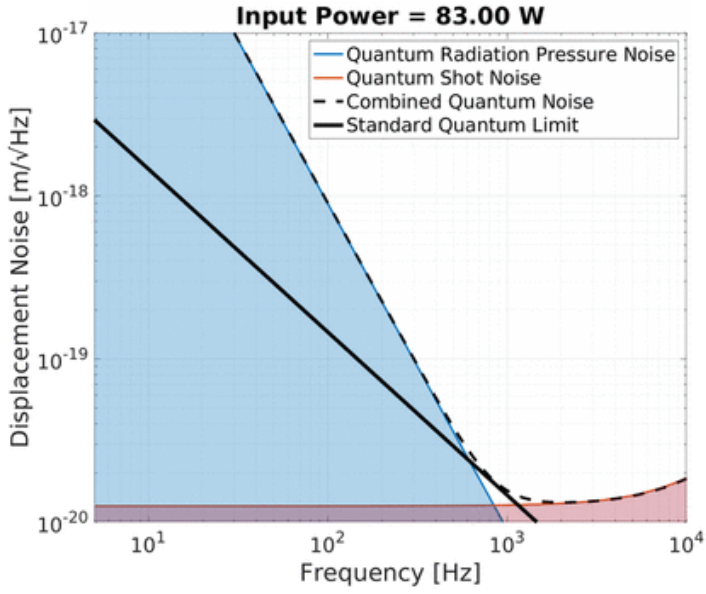

Figure: Shot + RP components and their sum vs frequency; SQL envelope.

Technical noises — at a glance

Noises to be kept a factor ~ 10 below the design sensitivity:

- Laser frequency noise
- Laser intensity noise
- Laser beam jitter
- Alignment fluctuations
- Scattered light
- Residual gas (phase noise, acoustic coupling)
- Control-loop noise
- Electronic noise (ADC, photodiodes)
- Magnetic field coupling
- Calibration lines and hardware injections

Key principle

Each of these is individually a major engineering effort. The art of detector commissioning is characterizing and suppressing all of them simultaneously.

Reading a real noise budget

How to read the figure:

- Thick line: total sensitivity.
- Coloured lines: individual contributions.
- Where total $\simeq$ one component: detector is limited by that noise.
- Where total $>$ sum of known contributions: unidentified noise ($\rightarrow$ work to do).
- Narrow lines: resonances (violin modes, suspensions, calibration).

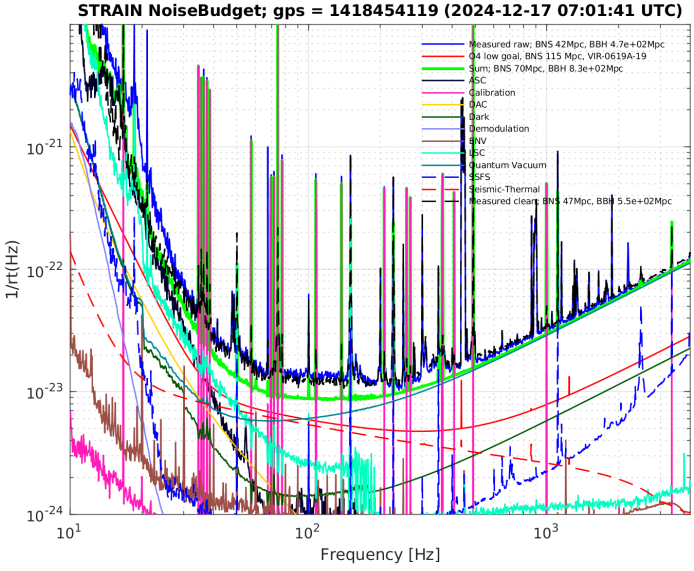

Figure: AdV noise budget (exp).

D. From strain sensitivity to astrophysical reach

- Astrophysical figure of merit: **horizon distance** or **BNS range** (distance at which a fiducial $1.4 + 1.4\,M_\odot$ binary gives SNR $= 8$).
- Scales roughly as $\int df\, |h_{\rm src}(f)|^2 / S_h(f)$.
- Typical advanced-detector ranges (O4):
  - LIGO Hanford / Livingston: ~ 150 Mpc;
  - Virgo: ~ 50–60 Mpc;
  - KAGRA: ~ 10 Mpc.
- Detection volume $\propto$ range^3 — doubling the range $\Rightarrow \times 8$ events.

The detector network

Currently operating / under construction (2G):

- **LIGO Hanford** (US, WA)
- **LIGO Livingston** (US, LA)
- **Virgo** (Italy, EGO)
- **KAGRA** (Japan, Kamioka)
- **LIGO-India** (under construction)

Next generation (3G):

- **Einstein Telescope** (Europe, site TBD)
- **Cosmic Explorer** (US)

→ ***M. Punturo*** *— 3G observatories and ET (Thu 21, 14:30);* ***W.J. Weber*** *— Space-based detectors (Thu 21, 16:35);* ***B. Patricelli*** *— Scientific achievements of current detectors (Wed 27, 16:35).*

Figure: World map with detector locations marked.

Antenna patterns of a network — sky coverage

- Single detector: quadrupolar pattern.
- Two detectors: still major blind zones.
- Three or more, at different latitudes/orientations: *nearly uniform* sky coverage.
- Network SNR:

$$\mathrm{SNR}^2_{\mathrm{net}} = \sum_a \mathrm{SNR}^2_a.$$

- Polarization reconstruction requires *at least three* detectors with non-degenerate orientations.

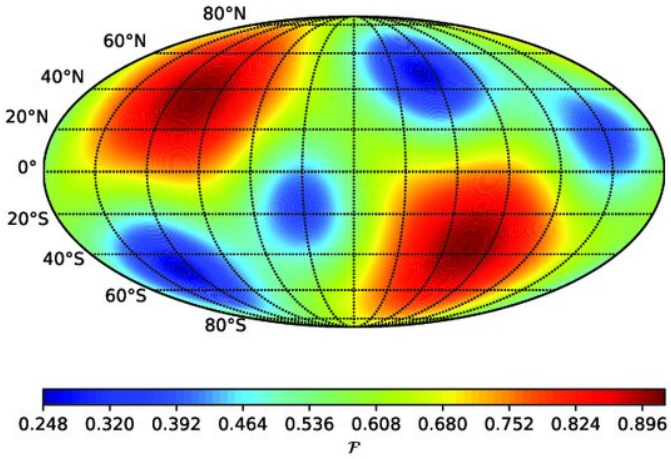

Figure: Sky map: 3-det antenna patterns.

Sky localization — triangulation

- Arrival-time differences between detectors $\rightarrow$ source direction.
- Angular resolution scales as

$$\Delta\Omega \propto \frac{1}{(\mathrm{SNR})^2 \cdot \Delta t^2_{\mathrm{baseline}}}.$$

- Longer baselines $\Rightarrow$ better localization:
  - LIGO-Virgo: $\sim$ 10 ms baselines.
  - Adding KAGRA and LIGO-India: $\sim$ 30 ms.
- Critical for multi-messenger follow-up (GW170817).

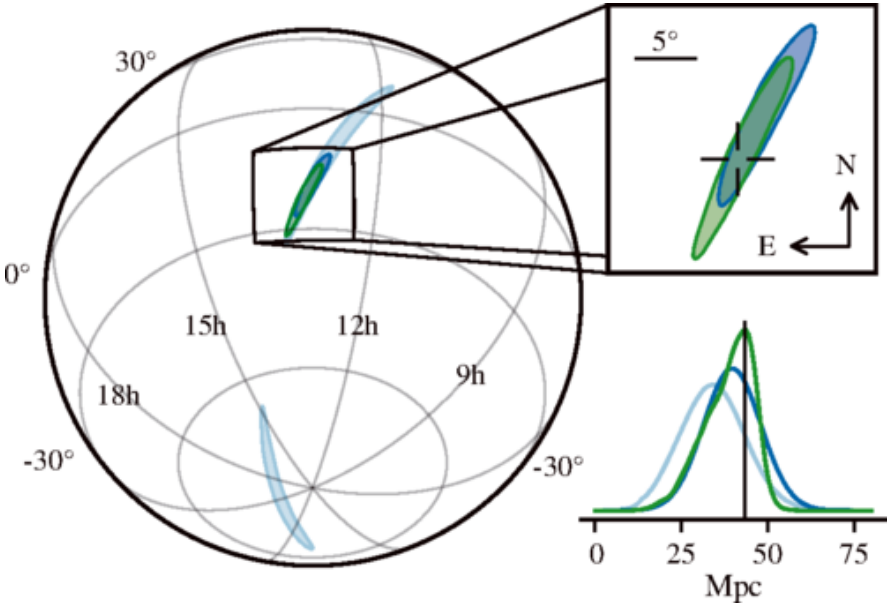

Figure: Sky location reconstructed for GW170817 .

What comes next in the school

Topics we touched on only briefly, covered in dedicated lectures:

- Optical configurations (Fabry-Perot, dual recycling, signal extraction) — **A. Perreca** (Fri 22, Sat 23)
- Control systems and length/alignment sensing — **D. Bersanetti** (Sat 23)
- Quantum noise and squeezing in depth — **F. Sorrentino** (Tue 26)
- Suspension design and seismic isolation — **P. Chessa** (Fri 22)
- Coating and mirror technology — **M. Magnozzi** (Fri 22)
- Laser technologies — **M. Galimberti** (Mon 25); stray light — **L. Conti** (Mon 25, Tue 26)
- Cryogenics — **E. Majorana** (Wed 27); thermal compensation — **I. Nardecchia** (Mon 25)
- Data analysis: matched filtering, parameter estimation, unmodelled searches — **F. Pannarale** (Tue 26, Wed 27)
- **Third-generation detectors**: Einstein Telescope and Cosmic Explorer — **M. Punturo** (Thu 21); space-based — **W.J. Weber** (Thu 21), **G. Wanner** (Fri 22)

Block 2 — Summary

- **Michelson** is the natural topology for a differential length measurement.
- **Fabry-Perot + power recycling**: bring shot noise to usable levels.
- **Noise budget**: seismic & Newtonian at LF, thermal in the middle, quantum at HF.
- **Sensitivity curve** is the designer's map: each region has a different physics driver.
- **Network** is essential for sky localization and polarization reconstruction.

Take-away

A GW detector is a multi-km precision machine where *every* noise source has been pushed to the limit allowed by known physics.

Key equations to leave with

1. GW-induced phase shift in a Michelson: $\Delta\varphi_{\rm gw} = \dfrac{4\pi L}{\lambda_L}\, h$.
2. Shot-noise-limited strain: $h_{\rm shot} \propto \dfrac{1}{L\sqrt{P_{\rm circ}}}$.
3. FP arm cavity gain: $L_{\rm eff} \simeq \frac{2\mathcal{F}}{\pi}\, L, \quad f_{\rm pole} = \frac{c}{4\mathcal{F}L}$.
4. Pendulum isolation: $x_{\rm mass}/x_{\rm ground} \simeq (f_0/f)^2$.
5. Standard Quantum Limit: $S_h^{\rm SQL}(f) = \dfrac{8\hbar}{mL^2\,(2\pi f)^2}$.

Further reading — Block 2 I

[1] Massimo Bassan, ed. *Advanced Interferometers and the Search for Gravitational Waves*. Vol. 404. Astrophysics and Space Science Library. Cham: Springer, 2014. ISBN: 978-3-319-03791-2. DOI: 10.1007/978-3-319-03823-0.

[2] Michele Maggiore. *Gravitational Waves. Vol. 1: Theory and Experiments*. Oxford: Oxford University Press, 2007. ISBN: 978-0-19-857074-5. DOI: 10.1093/acprof:oso/9780198570745.001.0001.

[3] Peter R. Saulson. *Fundamentals of Interferometric Gravitational Wave Detectors*. 2nd ed. Singapore: World Scientific, 2017. ISBN: 978-981-314-307-4. DOI: 10.1142/9book.

[4] J. Aasi et al. "Advanced LIGO". In: *Classical and Quantum Gravity* 32.7 (2015), p. 074001. DOI: 10.1088/0264-9381/32/7/074001. arXiv: 1411.4547.

[5] F. Acernese et al. "Advanced Virgo: a second-generation interferometric gravitational wave detector". In: *Classical and Quantum Gravity* 32.2 (2015), p. 024001. DOI: 10.1088/0264-9381/32/2/024001. arXiv: 1408.3978.

Further reading — Block 2 II

[6] T. Akutsu et al. "Overview of KAGRA: Detector design and construction history". In: *Progress of Theoretical and Experimental Physics* 2021.5 (2021), 05A101. DOI: 10.1093/ptep/ptaa125. arXiv: 2005.05574.

[7] Adrian Abac et al. "The Science of the Einstein Telescope". In: *arXiv e-prints* (2025). arXiv: 2503.12263 [gr-qc].

End of Block 2

Thank you!

Questions and discussion

Gianluca Gemme — INFN Sezione di Genova
gianluca.gemme@ge.infn.it